

Efficient implementation of randomized quantum algorithms with dynamic circuits

Shu Kanno,^{1,2,*} Ikko Hamamura,^{3,†} Rudy Raymond,^{2,3,‡} Qi Gao,^{1,2} and Naoki Yamamoto^{2,4}

¹*Mitsubishi Chemical Corporation, Science & Innovation Center,
1000, Kamoshida-cho, Aoba-ku, Yokohama 227-8502, Japan*

²*Quantum Computing Center, Keio University, Hiyoshi 3-14-1, Kohoku, Yokohama 223-8522, Japan*

³*IBM Quantum, IBM Research – Tokyo, 19-21 Nihonbashi Hakozaiki-cho, Chuo-ku, Tokyo 103-8510, Japan*

⁴*Department of Applied Physics and Physico-Informatics, Keio University,
3-14-1 Hiyoshi, Kohoku-ku, Yokohama, Kanagawa 223-8522, Japan*

Randomized algorithms are crucial subroutines in quantum computing, but the requirement to execute many types of circuits on a real quantum device has been challenging to their extensive implementation. In this study, we propose an engineering method to reduce the executing time for randomized algorithms using dynamic circuits, i.e., quantum circuits involving intermediate measurement and feedback processes. The main idea is to generate the probability distribution defining a target randomized algorithm on a quantum computer, instead of a classical computer, which enables us to implement a variety of static circuits on a single dynamic circuit with many measurements. We applied the proposed method to the task of random Pauli measurement for one qubit on an IBM superconducting device, showing that a 14,000-fold acceleration of executing time was observed compared with a conventional method using static circuits. Additionally, for the problem of estimating expectation values of 28- and 40-qubit hydrogen chain models, we successfully applied the proposed method to realize the classical shadow with 10 million random circuits, which is the largest demonstration of classical shadow. This work significantly simplifies the execution of randomized algorithms on real quantum hardware.

I. INTRODUCTION

Randomized algorithms are important subroutines in quantum computing. Their applications span a wide range of areas, including expectation value calculations [1, 2], error mitigation [3], time evolution [4, 5], and circuit cutting [6, 7]. Here, we take the classical shadow [1] as an example. The classical shadow is a technique that calculates expectation values of M (local) observables using $O(\log M)$ measurements through random measurements. For instance, in quantum chemistry calculations, the number of Pauli terms in a Hamiltonian scales as $O(N_{\text{so}}^4)$, and thus the classical shadow can suppress the polynomial growth in the number of measurements due to $O(\log N_{\text{so}}^4) = O(\log N_{\text{so}})$, where N_{so} is the number of spin orbitals.

However, execution time is a major obstacle to validating randomized algorithms on real devices. This is because randomized algorithms require the execution of a huge variety of circuits generated from a probability distribution. For example, in the classical shadow using single-qubit Clifford operations, qubits in a circuit are randomly measured in the X , Y , or Z bases according to the uniform distribution for each shot. However, under a fixed number of circuit executions, performing many shots on a single circuit is faster than executing one shot for each of multiple circuits, due to the compilation process of each circuit [8]. Concretely, the basic

execution capacity on an IBM device had been limited to 300 circuits per job, whereas 100,000 shots per circuit are allowed [9] (while recently the limitation seems to have been alleviated [10]). Consequently, executing a large number of circuits requires splitting them across multiple jobs. Even experiments with a few qubits would require about 10^4 circuits [11–13], and each job can take tens of minutes to hours [9], preventing such randomized algorithm from becoming practical. Note that, while the circuit stitching which executes multiple circuits using qubit reset and restart [14] may reduce the runtime, it still requires compilation for each of the circuits. Thus, too much execution time is a substantial obstacle to the validation of randomized algorithms on real devices.

To address this engineering challenge, we propose an accelerated implementation method of randomized quantum algorithms. Our idea is based on the dynamic circuit [15], which is a protocol involving mid-circuit measurements with feedback, commonly used in applications such as error correction. An overview of our approach is shown in Fig. 1, where we depict the case of random Pauli measurement. In conventional methods shown in the upper panel, multiple circuits to be executed are first determined classically according to the probability distribution corresponding to a target randomized algorithm, and they are each executed with one (or a few) shot(s) on a quantum computer. In contrast, our proposed method shown in the lower panel uses only a single dynamic circuit. This circuit first generates the probability distribution in the quantum register state and temporarily stores the measurement results in classical registers (G in the figure); the stored results are fed back to the quantum registers (F) for the re-initialized state (U_p with qubit reset). The values stored in the classical register vary for

* shu.kanno@quantum.keio.ac.jp

† S.K. and I.H. contributed equally to this work.; Present Address: NVIDIA G.K., Tokyo 107-0052, Japan.

‡ R.R. is an advisor to WPI Bio2Q of Keio Univ., Tokyo 160-8582, Japan.

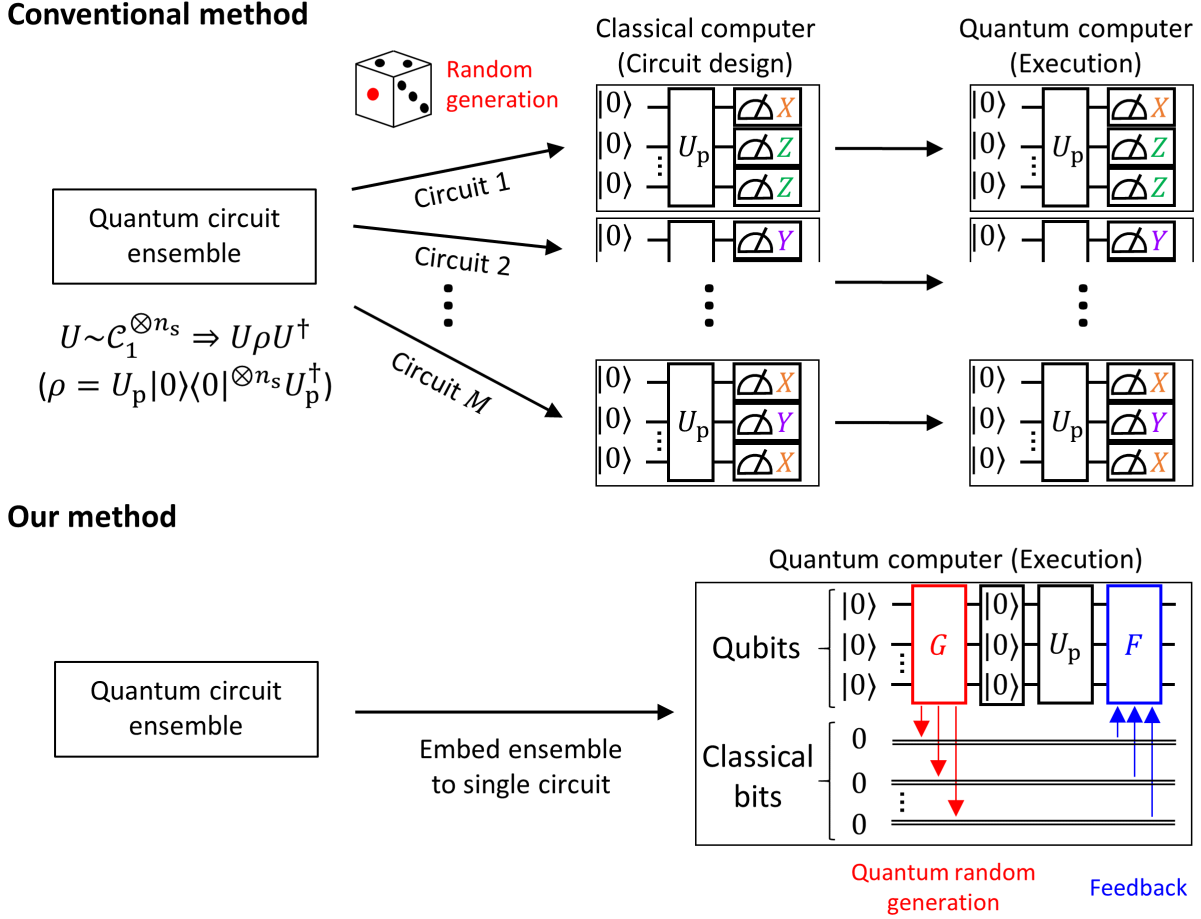


FIG. 1. Overview of our method for the case of random Pauli measurement. \mathcal{C}_1 is a single-qubit Clifford group, and n_s is the number of qubits. Single lines and double lines in the quantum circuits represent quantum and classical registers (bits), respectively. The conventional methods randomly generate multiple static circuits and execute each of them with one (or a few) shot(s) on a quantum computer. In contrast, the proposed method executes a single dynamic circuit multiple times.

each shot, enabling the execution of different static circuits for each shot on a single dynamic circuit. Since the circuit submitted to the device is a single dynamic circuit, the compilation is only one time, which allows for rapid sampling of a large number of types of static circuits exceeding the circuit limit that can be packed into a single job. Therefore, the proposed method would enable a drastic reduction of the total execution time for randomized algorithms.

The rest of this paper is composed as follows. The technical details of our method are explained in Sec. II. Verification for the single-qubit random Pauli measurement is shown in Sec. III A. Energy calculations for chemical models by using the classical shadow are demonstrated in Sec. III B. Conclusions and outlooks are stated in Sec. IV.

II. METHODS

A high-level sketch of a circuit in our method is shown in Fig. 2(a), where the circuit is composed of n_s sys-

tem qubits, n_a ancilla qubits, and n_c classical bits. We first encode the probability distribution corresponding to a target randomized algorithm, to a quantum state; we measure them and record the results on classical bits (G , red in the figure). Then, we execute conditional feedback operations based on the measured results (F , blue in the figure). Given a fixed number of circuit executions, executing an identical circuit with multiple shots is faster than executing many different circuits with one (or a few) shot, and thus our method is expected to run randomized algorithms with much less time compared to the conventional methods. As a specific case of $n_s = n_a$, the system and ancilla qubits are shared by using the qubit reset technique in Fig. 2(b). In the next section, we adopt this circuit, because it can reduce not only the number of qubits but also possible noise affections on the system qubits during the idle time (i.e., the period of executing on G) in the case of Fig. 2(a).

Let us consider a detail of the circuit Fig. 2(a), which is shown as Fig. 2(c). The circuit includes S slots $\{F_1, \dots, F_S\}$ and each slot F_j randomly executes one of

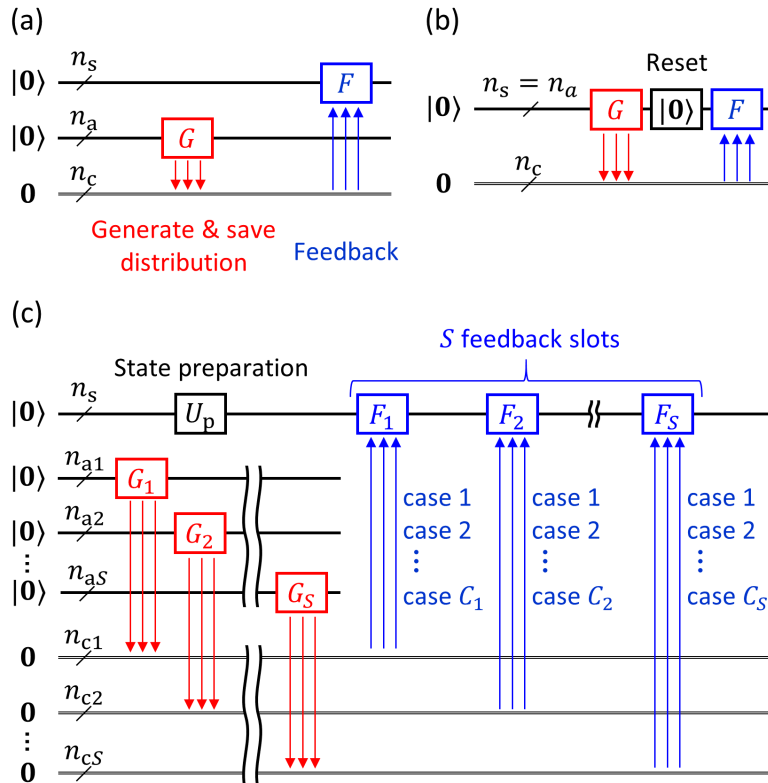


FIG. 2. Depictions of the proposed method. Single lines and double lines represent quantum and classical registers, respectively. (a) Abstract circuit diagram. (b) Qubit saving version. (c) Detailed circuit diagram. In (a), the first single line represents system qubits and the second single line represents ancilla qubits, while the system and ancilla qubits are shared in (b).

the C_j gate operations depending on the measurement result on G_j . Corresponding to each F_j , we assume to use n_{aj} qubits for generating the probability distribution that is the output of G_j , where $n_a = \sum_{j=1}^S n_{aj}$. The distribution can be encoded either analytically or numerically, for example, using a variational procedure [16] for the latter case. The measurement result is stored in the n_{cj} classical bit, where $n_c = \sum_{j=1}^S n_{cj}$. Note that n_a and n_c are at most $S \lceil \max_j (\log_2(C_j)) \rceil$. Here, we depicted a state preparation gate U_p to make it easier to understand while it can be generally included in F_1 .

We can efficiently execute the circuit when both S and C_j are $\mathcal{O}(\text{poly}(n_s))$; note that if $S = \Omega(e^{n_s})$ and $C_j = \Omega(e^{n_s})$, the circuit depth the classical computational time would become exponential, respectively. One executable example is the random compiler for the Hamiltonian simulation suitable for chemical models, called qDRIFT [4]; if the target Hamiltonian H is of the form $H = \sum_{i=1}^L h_i H_i$ with h_i a positive real coefficient and H_i a Hermitian operator (e.g., Pauli string), then S and C_j scale as $(\sum_{i=1}^L h_i)^2 = \mathcal{O}(\text{poly}(n_s))$ and $L = \mathcal{O}(\text{poly}(n_s))$, respectively. On the other hand, the n_s -qubit random Clifford version naively takes $C_j = \mathcal{O}(2^{\text{poly}(n_s)})$, and thus the efficient procedure for the implementation remain open; the sophisticated procedure for choice of the

random operation would be required [17, 18]. Yet, the classical shadow with single-qubit random Clifford unitaries can also be executed since $S = n_s$ and $C_j = 3$ due to the Pauli X, Y and Z basis measurements, which is demonstrated in the next section.

Finally, it is worth noting that while the proposed method aims more at engineering algorithm acceleration than quantum advantage, we can assume possible scenarios for such advantage. An example is the case of randomized algorithms operating on probability distributions governed by a quantum state (e.g., the state of Eq. (1) in the next section) that can be effectively generated only on quantum circuits [19–21]. Additionally, there might be an advantage if there is a significant difference between classically generated pseudo-random numbers and true random numbers generated by quantum computers.

III. RESULTS AND DISCUSSIONS

A. Verification with random measurement for single qubit

First, we demonstrate our method with the random measurements in the X, Y , and Z bases for a single

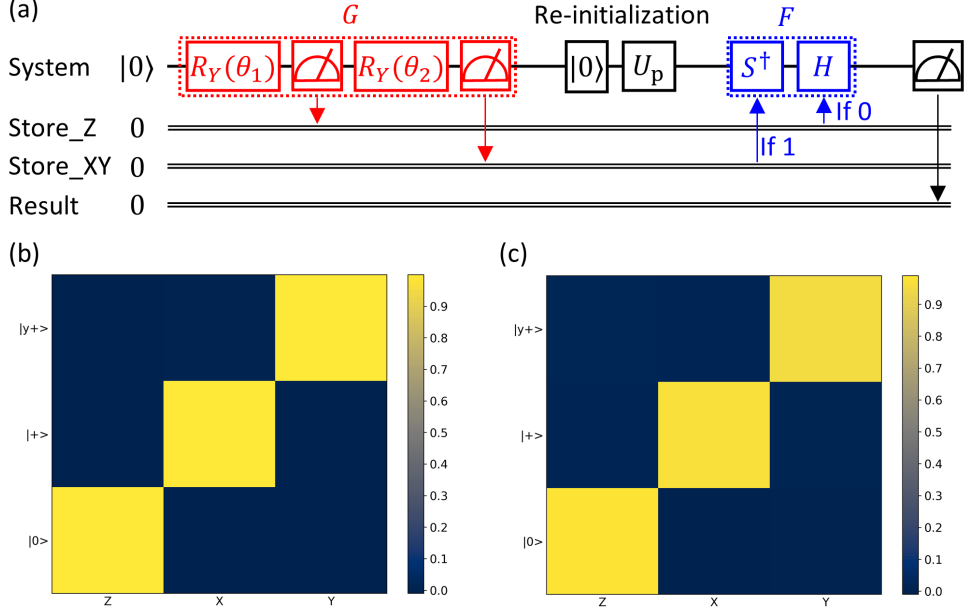


FIG. 3. One qubit test for the random Pauli measurement. (a) Circuit for the verification. The single line and double lines represent quantum and classical registers, respectively. The rectangle areas surrounded by red and blue dotted lines represent G and F , respectively. (b) and (c) show the contour plots for the expectation values of Z , X , and Y for respective initialized states $|0\rangle$, $|+\rangle$, and $|y+\rangle$. (b) State vector simulator results. (c) Real device results (*ibmq.kolkata*).

qubit. Figure 3(a) shows the constructed circuit. This circuit consists of one quantum and three classical registers. The system and ancilla qubits are shared as in Fig. 2(a) ($n_s = n_a = 1$). The first two classical registers store the probability distribution ($n_c = 2$), and the last classical register stores a result to calculate expectation values.

While we can consider the implementation with $S = 1$ and $C_1 = 3$ like Fig. 2(c), we here implement the circuit that involves less feedback operations, as follows. The RY gate operation followed by measurement are repeated twice at the beginning, with the first- and second-measurement results stored in the classical registers “Store_Z” and “Store_XY”, respectively (red in Fig. 3(a)).

More precisely, we set the rotation angles of the two RY gates to $\theta_1 = 2 \arccos \sqrt{2/3}$ and $\theta_2 = 2 \arccos \sqrt{1/2}$, which generates $|\phi_1\rangle$ followed by $|\phi_2\rangle$:

$$|\phi_1\rangle = \sqrt{\frac{2}{3}}|0\rangle + \sqrt{\frac{1}{3}}|1\rangle, \quad |\phi_2\rangle = \pm\sqrt{\frac{1}{2}}|0\rangle + \sqrt{\frac{1}{2}}|1\rangle, \quad (1)$$

where plus (minus) sign appears in $|\phi_2\rangle$ when $|0\rangle$ ($|1\rangle$) was measured in the first measurement of $|\phi_1\rangle$. The probabil-

ities of the measurement result are given by

$$\begin{aligned} \Pr(\text{Store_Z} = 0, \text{Store_XY} = 0) &= \frac{2}{3} \cdot \frac{1}{2} = \frac{1}{3}, \\ \Pr(\text{Store_Z} = 0, \text{Store_XY} = 1) &= \frac{2}{3} \cdot \frac{1}{2} = \frac{1}{3}, \\ \Pr(\text{Store_Z} = 1, \text{Store_XY} = 0) &= \frac{1}{3} \cdot \frac{1}{2} = \frac{1}{6}, \\ \Pr(\text{Store_Z} = 1, \text{Store_XY} = 1) &= \frac{1}{3} \cdot \frac{1}{2} = \frac{1}{6}. \end{aligned}$$

Next, the state is reset, and an initial state $|\psi\rangle$ is generated by U_p . Then, corresponding to the above measurement results from top to bottom, we apply H, HS^\dagger, S^\dagger , and I to $|\psi\rangle$, respectively (blue in Fig. 3(a)). Finally, we measure Z , meaning that we make the measurement of X, Y, Z , and Z , respectively, corresponding to the above (pre)measurement result, because of $HZH = X$, $SHZHS^\dagger = Y$, $SZS^\dagger = Z$, and $IZI = Z$. As a consequence,

$$\begin{aligned} \Pr(\text{measure } X) &= \Pr(\text{Store_Z} = 0, \text{Store_XY} = 0) = \frac{1}{3}, \\ \Pr(\text{measure } Y) &= \Pr(\text{Store_Z} = 0, \text{Store_XY} = 1) = \frac{1}{3}, \\ \Pr(\text{measure } Z) &= \Pr(\text{Store_Z} = 1) = \frac{1}{3}, \end{aligned}$$

thus we realize the random measurement of X, Y, Z with equal probability $1/3$.

Finally, the measured result is stored in the classical

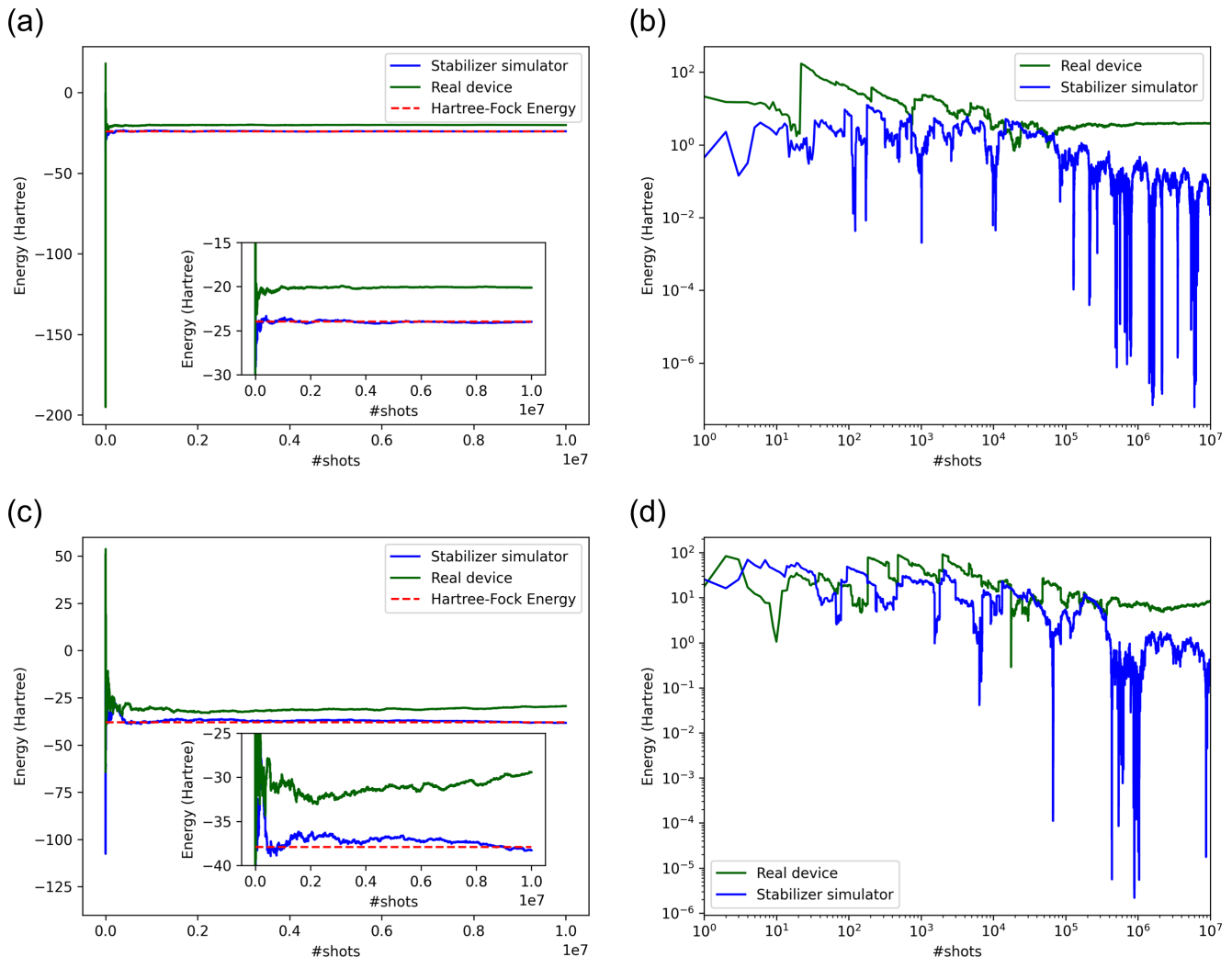


FIG. 4. Results of expectation values for the hydrogen chain model with Hartree-Fock state. (a) and (b) [(c) and (d)] are the results for 28 [40] qubits. (a) and (c) show the exact values of energy (Hartree-Fock energy) $\langle \text{HF} | H | \text{HF} \rangle$ as well as the estimated values via the real devices and the simulator. For the real device experiment, the readout error mitigation was not carried out. The insets are enlarged views of the y-axis. (b) and (d) show the results of differences between the exact values and the estimated values in the log-log plot. We adopt *ibm_kawasaki* and *ibm_kyiv* devices for the cases of 28 and 40 qubits demonstration, respectively.

bit “Result”. We can estimate the expected value for the randomized measurement by using the selected basis stored in `Store_Z` and `Store_XY` in addition to the measured result in `Result`. Note that if the ratio of measurement bases needs to be changed, which happens in the Locally-Biased Classical Shadow [2] for example, it can be adjusted by modifying the RY rotation angles.

We calculate the expectation values $\langle Z \rangle$, $\langle X \rangle$, and $\langle Y \rangle$ based on their respective eigenstates $|0\rangle$, $|+\rangle$, and $|y+\rangle$ using $U_p = I, H$, and $R_X(-\pi/2)$. The whole quantum computations were conducted based on Qiskit [22]. The results obtained using the QASM simulator and the real device *ibmq_kolkata* are presented in Figs. 3(b) and (c), respectively. The values in each row were obtained by

executing a single type of dynamic circuit for 100,000 shots. In both the figures, only the expectation values corresponding to the eigenstates are almost 1, while the others are almost 0. The execution time for these 100,000 quantum circuits was 40 seconds, which is obtained from the value of `time_taken` in a result output. For comparison with the conventional approach, we executed 100 random measurement circuits by 1 shot for 100 jobs; then the execution took 540 seconds. Therefore, the proposed method achieved a speedup of $\frac{100000}{40} / \frac{100}{540} \approx 14,000$ times.

We comment on the potential for further accelerations. In our current setup, each job contained only a single circuit. Allowing the execution of multiple circuits per job could lead to additional speedups. However, IBM’s im-

posed instruction count limit [10] — which heavily penalizes certain operations, such as measurement and reset — poses challenges for scaling this approach. As a result, as shown in later sections, we were forced to limit each job to one circuit and reduce the number of shots in some cases due to the limitation. Nevertheless, this limitation may be temporary. Dynamic circuits were introduced primarily to support error correction, suggesting that these restrictions could be relaxed in the future. Furthermore, recently introduced batch jobs, i.e., parallel compilation as described in the following section offer another avenue for accelerating computation [23].

B. Large scale demonstrations

Here we demonstrate the effectiveness of our method on relatively large-scale chemical problems. Specifically, we calculated the expectation values of Hamiltonians of hydrogen models, using the classical shadow with random Pauli measurement. We study the model of (14e, 14o) and (20e, 20o), corresponding to 28 and 40 qubits, respectively, where (Ae , Bo) represents A electrons and B orbitals in a chemical model. The 28 (40) qubit hydrogen chain model was created by arranging 14 (20) hydrogen atoms at one angstrom interval. The STO-3G basis set was used. The constructed second-quantized Hamiltonian H is represented as

$$H = \sum_{ij} c_{ij} a_i^\dagger a_j + \sum_{ijkl} c_{ijkl} a_i^\dagger a_j^\dagger a_l a_k, \quad (2)$$

which is transformed into a qubit Hamiltonian as

$$H = \sum_I C_I P_I, \quad (3)$$

where c_{ij} , c_{ijkl} , and C_I are coefficients, a_i (a_i^\dagger) is creation (annihilation) operator, and P_I is a Pauli string. The second-quantized Hamiltonian was constructed from the result of the Hartree–Fock calculation, which was transformed by the Bravyi–Kitaev transformation to obtain the qubit Hamiltonian. The state in the re-initialization is the Hartree–Fock state; $|\text{HF}\rangle = U_p |0\rangle^{\otimes n_s}$.

To estimate the expectation value $\langle H \rangle = \sum_I C_I \langle P_I \rangle$, in the Pauli-based classical shadow formalism $\langle P_I \rangle$ is calculated as the mean of $\text{Tr}(P_I \hat{\rho})$ with $\hat{\rho}$ a random state called the snapshot:

$$\hat{\rho} = \bigotimes_{i=1}^n \left[3U_i^\dagger |b_i\rangle \langle b_i| U_i - I \right].$$

U_i randomly takes the single-qubit Pauli operator X , Y , or Z with equal probability $1/3$, and $\bigotimes_i |b_i\rangle$ is the projected computational basis state obtained as a result of measuring $\bigotimes_i U_i |HF\rangle$. We construct the quantum circuit together with the classical register as a straightforward extension of that studied in the previous subsection; i.e.,

product of the circuit shown in Fig. 3(a). The detail of the circuit configuration for the 28 and 40 qubits are shown in Appendix A. We used the Eagle devices, specifically *ibm_kawasaki* and *ibm_kyiv* for 28 and 40 qubit models, where the numbers of shots (i.e., the numbers of snapshots) per job are 100,000 and 50,000, respectively. Again, we emphasize that only one circuit was packed for each job. A single job took around 30 minutes while we partially used the batch jobs to reduce the total runtime. The optimization level for a circuit was three. We also classically performed the state preparation and the random Pauli measurement using a stabilizer simulator on Qiskit for the noiseless reference. Note that although the qubits are not entangled to compare the results with the noiseless references, we can trivially use the entangled initial state by adding two-qubit gates in U_p .

Figure 4 shows the results of $\langle H \rangle$. The figures (a) and (c) represent the energy values for the 28- and 40-qubit models, respectively. For both models, the classically calculated values via the stabilizer simulator (blue line) fluctuate around the true Hartree–Fock energy $\langle H \rangle = \langle \text{HF} | H | \text{HF} \rangle$ (red dashed line) as the number of shots increases. The mean values with standard deviations for the 28- and 40-qubit models using the results between 10^6 to 10^7 shot counts are -24.008 ± 0.103 and -37.248 ± 0.462 Hartree, where Hartree–Fock energies are -23.975 and -37.910 Hartree, respectively. Figures 4(b) and (d) show the absolute error from the Hartree–Fock energy for the 28- and 40-qubit models, respectively. In both models, as the number of shots increases, the errors tend to decrease. However, the error remains orders of Hartree, much larger than the chemical precision (≈ 0.0016 Hartree). Also, the error in the 40-qubit model is larger than that in the 28-qubit model. The increase of locality in Pauli terms and the norm of a qubit Hamiltonian would be a cause of decreasing precision. It is noted that faster convergence could be achieved through more sophisticated qubit mappings or randomized methods [2, 24–26] while this is out of scope in this study as the focus is on accelerating real-device implementation.

The real device results are shown by green lines in the figures, where the mean values are -20.091 ± 0.054 and -31.113 ± 0.803 Hartree for the 28- and 40-qubit models, respectively. Certainly, Figs. 4(a) and (b) show that there is a deviation from the true value. However, Figs. 4(c) and (d) indicate that the values converge around after 10^6 shots. This convergence behavior becomes apparent in the regime of many sampling, which is in our case over 10^6 sampling, highlighting an important insight enabled by the acceleration of the random algorithm in this study.

Finally, we mention that we executed a readout error mitigation for these results to reduce the biases; see Fig. 8 in Appendix B. The estimated values of energy via our method for 28 and 40 qubit models are -20.111 ± 0.056 and -31.475 ± 1.118 Hartree, 20 and 362 milli Hartree reduction from the original results, respectively. However, the large biases still remained, and thus the other types of errors such as the initialization, one-qubit gate, and

dephasing errors, should be mitigated to obtain more accurate results.

IV. CONCLUSIONS

We proposed a dynamic-circuit-based method to efficiently execute randomized algorithms on real quantum devices. This method consists of generating the probability distribution in the amplitude of a quantum register state, recording the results in the classical register via measurement, and feeding them back to the quantum register to realize the randomized algorithm. We applied the proposed method to verify a one-qubit randomized Pauli measurement and found 14,000 times acceleration compared to the conventional method. The one-qubit randomized Pauli measurement can be utilized to realize the classical shadow method for observable estimation. We particularly computed Hartree–Fock energies for 28- and 40-qubit hydrogen chain models using the classical shadow on real devices. The method was successfully executed up to 10^7 shots; this number of random circuit sampling is the largest compared with the previous studies [9, 11–13, 27, 28].

Since randomized algorithms are utilized in a wide range of quantum algorithms, the applications of the proposed method are numerous. For example, potential applications in error mitigation include gate error mitigation techniques such as probabilistic error cancellation and readout error mitigation like twirled readout error extinction (TRES) [29–31]. Also, the early fault-tolerant quantum computing approaches often leverage Monte Carlo sampling to reduce gate costs, e.g., in the problem of calculating expectation values for time-evolved states [5]. Circuit cutting may also benefit from this acceleration, potentially enabling more two-qubit gates to be cut in practical scenarios.

Methods of embedding a probability distribution into a circuit are becoming increasingly important for various applications [16, 32, 33]. While conventional distribution embedding often assumes quantum variational algorithms, the proposed method may offer new insights because it allows classical distribution embeddings to a classically prepared shallow circuit [33–36]. As these methods are developing smoothly, we anticipate that dynamic-circuit-based approaches will accelerate existing quantum algorithms in various sense and open new pathways toward future quantum computing. Furthermore, it will open up the development of quantum algorithms that leverage probability distributions, which are difficult to generate classically.

V. DATA AVAILABILITY

The part of the codes and datasets in this study is available at https://github.com/sk888ks/Random_algorithm_dynamic_circuit_open.git.

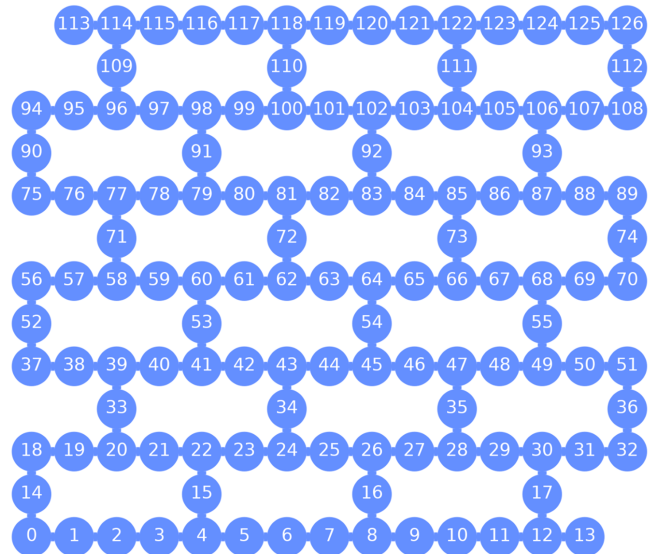


FIG. 5. Device topology of the Eagle devices.

ACKNOWLEDGMENTS

A part of this work was performed for Council for Science, Technology and Innovation (CSTI), Cross-ministerial Strategic Innovation Promotion Program (SIP), “Promoting the application of advanced quantum technology platforms to social issues”(Funding agency: QST). The part of calculations was performed on the Mitsubishi Chemical Corporation (MCC) high-performance computer (HPC) system “NAYUTA”, where “NAYUTA” is a nickname for MCC HPC and is not a product or service name of MCC. We acknowledge the use of IBM Quantum services for experiments in this paper. The views expressed are those of the authors, and do not reflect the official policy or position of IBM or the IBM Quantum team. This work was supported by the MEXT Quantum Leap Flagship Program under Grants No. JPMXS0118067285 and No. JPMXS0120319794.

Appendix A: Circuit in large scale executions.

Figure 5 shows the device topology of the Eagle devices. Figures 6 and 7 are circuit examples for 28 and 40-qubit models, respectively, where the qubit indices are shared with Fig. 5.

Appendix B: Results for a readout error mitigation.

We tried readout error mitigation based on the readout error from calibration data.

The algorithm used in the present paper is described as Algorithm 1. The notations here (specifically Q , α_Q , $f(P, Q)$, and $\mu(P, \text{supp}(Q))$) follow those of

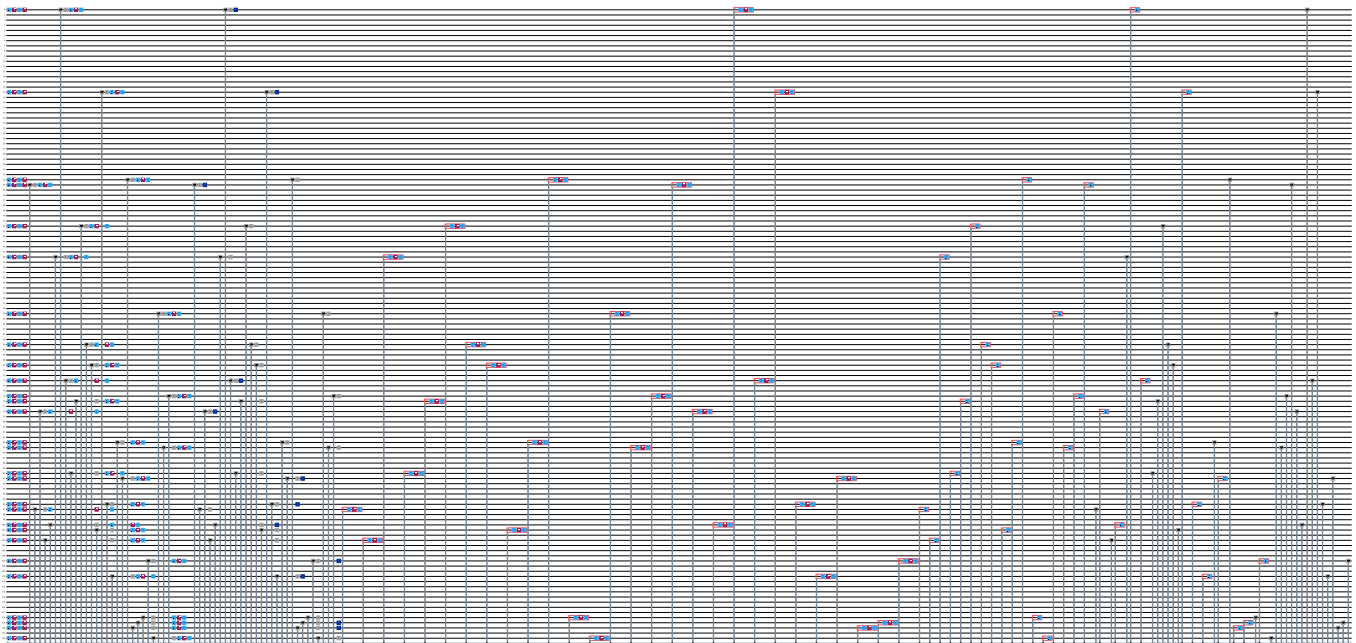


FIG. 6. Circuit example in the 28 qubit model.

Ref. [2]. Let the readout error for a qubit i be denoted as $e(i)$ and the corresponding factor is $m(i) = \frac{1}{1-2e(i)}$. This is based on the idea that, assuming a symmetric error on a single qubit, the reduction in the expectation value is $1 - 2e$. To restore the original expectation value, we multiply by its inverse. For a subset $A \subseteq \{1, 2, \dots, n\}$, $m(A)$ is defined as $m(A) = \prod_{i \in A} m(i)$

Figure 8 shows the results for the classical shadow before (green) and after (orange) the readout error mitigation. The improvement by the error mitigation was small. This could be due to differences in error rates between calibration and job execution, or the presence of significant correlated readout errors among multiple qubits. It is possible that the error during execution was larger than the error during calibration. To address this, it will be essential to measure the error rate during execution. Furthermore, by symmetrizing the errors, it should be possible to more efficiently estimate their impact on the estimation value [31]. Our quantum random number generator could also be leveraged in this measurement symmetrization process. This method takes account of the contribution of correlated errors through symmetrization.

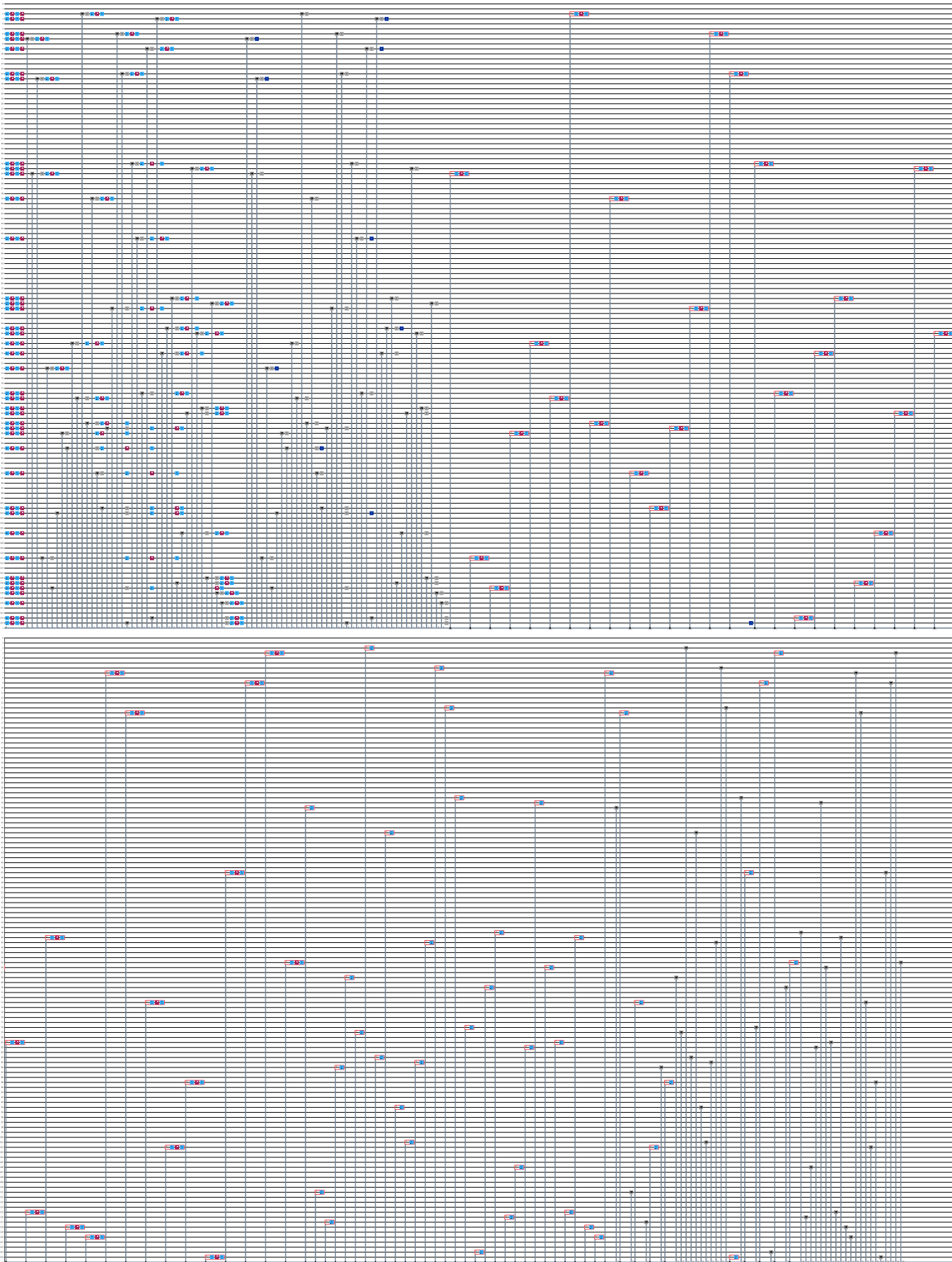


FIG. 7. Circuit example in the 40 qubit model.

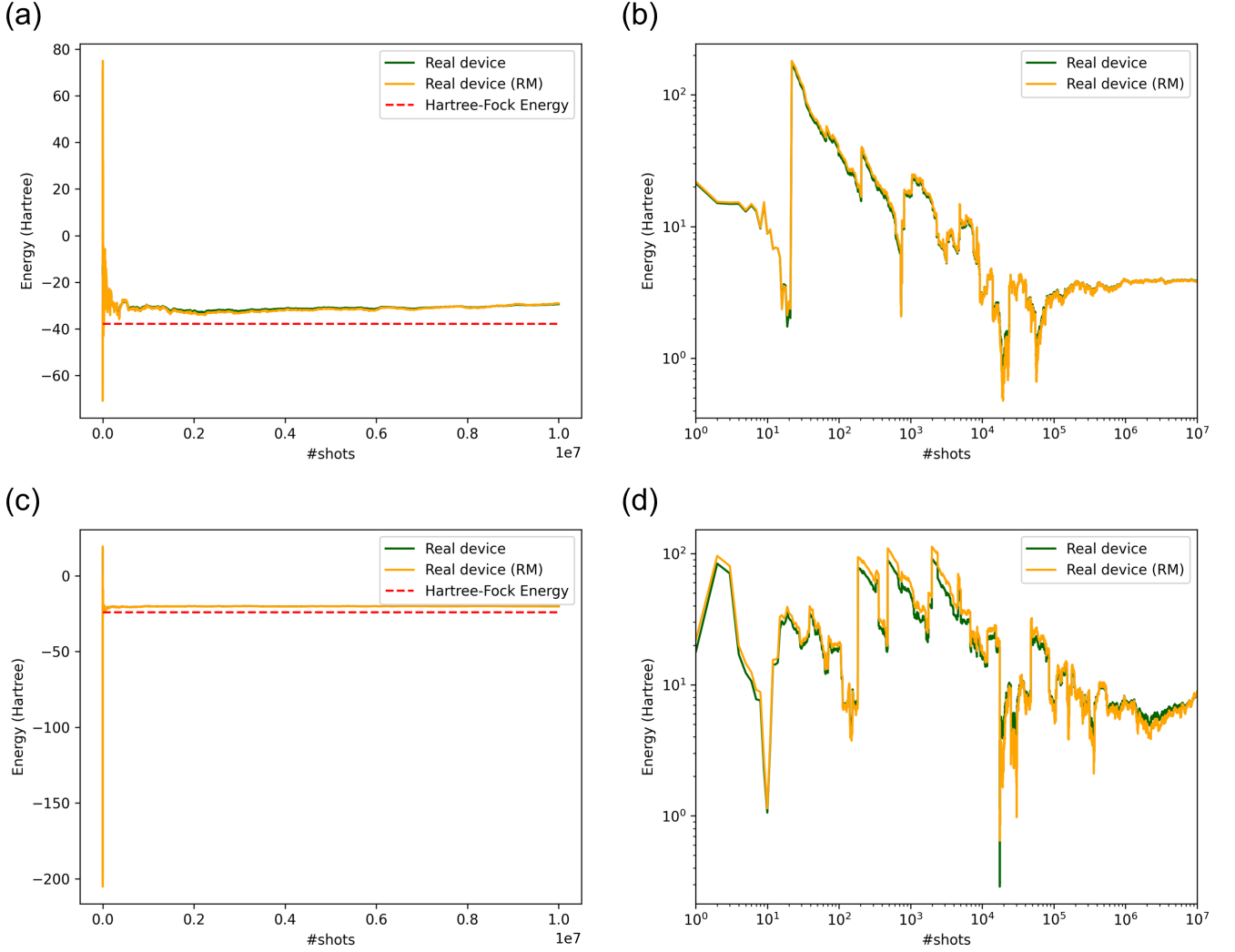


FIG. 8. Results of expectation values for the hydrogen chain model with Hartree–Fock state including the readout error mitigation. (a) and (b) [(c) and (d)] are the results for 28 [40] qubits. (a) and (c) show the exact values of energy (Hartree-Fock energy) $\langle \text{HF} | H | \text{HF} \rangle$ as well as the estimated values via the real devices with and without the readout error mitigation (RM). (b) and (d) show the results of differences between the exact values and the estimated values in the log-log plot. We adopt *ibm_kawasaki* and *ibm_kyiv* devices for the cases of 28 and 40 qubits demonstration, respectively.

Algorithm 1: Classical shadows with single qubit readout error mitigation

```

1 for all sample  $s \leftarrow \{1, 2, \dots, S\}$  do
2   Prepare state  $\rho$ ;
3   Random pick  $P \leftarrow \{X, Y, Z\}^{\otimes n}$ ;
4   for all qubit  $i \leftarrow \{1, 2, \dots, n\}$  do
5     Measure qubit  $i$  in  $P_i$  basis providing eigenvalue measurement  $\mu(P, i) \in \{\pm 1\}$ ;
6   Estimate expectation value

```

$$\nu^{(s)} = \sum_Q \alpha_Q m(\text{supp}(Q)) f(P, Q) \mu(P, \text{supp}(Q));$$

```

7 return  $\nu = \frac{1}{S} \sum_s \nu^{(s)}$ ;

```

- [1] H.-Y. Huang, R. Kueng, and J. Preskill, arXiv [quant-ph], 1050 (2020), 2002.08953.
- [2] C. Hadfield, S. Bravyi, R. Raymond, and A. Mezzacapo, arXiv [quant-ph] (2020), 2006.15788.
- [3] Z. Cai, R. Babbush, S. C. Benjamin, S. Endo, W. J. Huggins, Y. Li, J. R. McClean, and T. E. O'Brien, arXiv [quant-ph] (2022), 2210.00921.
- [4] E. Campbell, Phys. Rev. Lett. **123**, 070503 (2019).
- [5] Y. Yang, B.-N. Lu, and Y. Li, PRX quantum **2**, 040361 (2021).
- [6] T. Peng, A. W. Harrow, M. Ozols, and X. Wu, Phys. Rev. Lett. **125**, 150504 (2020).
- [7] H. Harada, K. Wada, and N. Yamamoto, PRX quantum **5**, 040308 (2024).
- [8] G. P. He, arXiv [quant-ph] (2023), 2307.08167.
- [9] K. Korhonen, H. Vappula, A. Glos, M. Cattaneo, Z. Zimborás, E.-M. Borrelli, M. A. C. Rossi, G. García-Pérez, and D. Cavalcanti, arXiv [quant-ph] (2024), 2409.02575.
- [10] Job limits, <https://docs.quantum.ibm.com/guides/job-limits/> (), accessed: 2025-1-30.
- [11] R. Levy, D. Luo, and B. K. Clark, Phys. Rev. Res. **6**, 013029 (2024).
- [12] T. Zhang, J. Sun, X.-X. Fang, X.-M. Zhang, X. Yuan, and H. Lu, Phys. Rev. Lett. **127**, 200501 (2021).
- [13] G. I. Struchalin, Y. A. Zagorovskii, E. V. Kovlakov, S. S. Straupe, and S. P. Kulik, PRX quantum **2** (2021).
- [14] Circuit stitching - H-series, https://docs.quantum.ibm.com/h-series/trainings/knowledge_articles/circuit_stitching.html#id1 (), accessed: 2025-1-30.
- [15] The full power of dynamic circuits to qiskit runtime, <https://www.ibm.com/quantum/blog/quantum-dynamic-circuits/> (), accessed: 2025-1-30.
- [16] K. Nakaji, S. Uno, Y. Suzuki, R. Raymond, T. Onodera, T. Tanaka, H. Tezuka, N. Mitsuda, and N. Yamamoto, Phys. Rev. Res. **4**, 023136 (2022).
- [17] R. Koenig and J. A. Smolin, J. Math. Phys. **55**, 122202 (2014).
- [18] E. van den Berg, arXiv [quant-ph] (2020), 2008.06011.
- [19] F. Arute, K. Arya, R. Babbush, D. Bacon, J. C. Bardin, R. Barends, R. Biswas, S. Boixo, F. G. S. L. Brandao, D. A. Buell, B. Burkett, Y. Chen, Z. Chen, B. Chiaro, R. Collins, W. Courtney, A. Dunsworth, E. Farhi, B. Foxen, A. Fowler, C. Gidney, M. Giustina, R. Graff, K. Guerin, S. Habegger, M. P. Harrigan, M. J. Hartmann, A. Ho, M. Hoffmann, T. Huang, T. S. Humble, S. V. Isakov, E. Jeffrey, Z. Jiang, D. Kafri, K. Kechedzhi, J. Kelly, P. V. Klimov, S. Knysh, A. Korotkov, F. Kostritsa, D. Landhuis, M. Lindmark, E. Lucero, D. Lyakh, S. Mandrà, J. R. McClean, M. McEwen, A. Megrant, X. Mi, K. Michielsen, M. Mohseni, J. Mutus, O. Naaman, M. Neeley, C. Neill, M. Y. Niu, E. Ostby, A. Petukhov, J. C. Platt, C. Quintana, E. G. Rieffel, P. Roushan, N. C. Rubin, D. Sank, K. J. Satzinger, V. Smelyanskiy, K. J. Sung, M. D. Trevithick, A. Vainsencher, B. Villalonga, T. White, Z. J. Yao, P. Yeh, A. Zalcman, H. Neven, and J. M. Martinis, Nature **574**, 505 (2019).
- [20] H.-S. Zhong, H. Wang, Y.-H. Deng, M.-C. Chen, L.-C. Peng, Y.-H. Luo, J. Qin, D. Wu, X. Ding, Y. Hu, P. Hu, X.-Y. Yang, W.-J. Zhang, H. Li, Y. Li, X. Jiang, L. Gan, G. Yang, L. You, Z. Wang, L. Li, N.-L. Liu, C.-Y. Lu, and J.-W. Pan, Science **370**, 1460 (2020).
- [21] D. Layden, G. Mazzola, R. V. Mishmash, M. Motta, P. Wocjan, J.-S. Kim, and S. Sheldon, Nature **619**, 282 (2023), 2203.12497.
- [22] A. Javadi-Abhari, M. Treinish, K. Krsulich, C. J. Wood, J. Lishman, J. Gacon, S. Martiel, P. D. Nation, L. S. Bishop, A. W. Cross, B. R. Johnson, and J. M. Gambetta, arXiv [quant-ph] (2024), 2405.08810.
- [23] Run jobs in a batch, <https://docs.quantum.ibm.com/guides/run-jobs-batch/> (), accessed: 2025-1-30.
- [24] S. B. Bravyi and A. Y. Kitaev, Ann. Phys. (N. Y.) **298**, 210 (2002).
- [25] C. Bertoni, J. Haferkamp, M. Hinsche, M. Ioannou, J. Eisert, and H. Pashayan, arXiv [quant-ph] (2022), 2209.12924.
- [26] A. Zhao, N. C. Rubin, and A. Miyake, Phys. Rev. Lett. **127**, 110504 (2021).
- [27] A. Elben, R. Kueng, H.-Y. R. Huang, R. van Bijnen, C. Kokail, M. Dalmonte, P. Calabrese, B. Kraus, J. Preskill, P. Zoller, and B. Vermersch, Phys. Rev. Lett. **125**, 200501 (2020).
- [28] W. J. Huggins, B. A. O'Gorman, N. C. Rubin, D. R. Reichman, R. Babbush, and J. Lee, Nature **603**, 416 (2022).
- [29] K. Temme, S. Bravyi, and J. M. Gambetta, Phys. Rev. Lett. **119**, 180509 (2017).
- [30] S. Endo, S. C. Benjamin, and Y. Li, Physical Review X (2018).
- [31] E. van den Berg, Z. K. Mineev, and K. Temme, Phys. Rev. A (Coll. Park.) **105**, 032620 (2022).
- [32] N. Mitsuda, T. Ichimura, K. Nakaji, Y. Suzuki, T. Tanaka, R. Raymond, H. Tezuka, T. Onodera, and N. Yamamoto, Phys. Rev. A **109**, 052423 (2024).
- [33] T. Shirakawa, H. Ueda, and S. Yunoki, Phys. Rev. Res. **6** (2024).
- [34] S.-J. Ran, Phys. Rev. A **101**, 032310 (2020).
- [35] M. S. Rudolph, J. Chen, J. Miller, A. Acharya, and A. Perdomo-Ortiz, arXiv [quant-ph] (2022), 2209.00595.
- [36] S. Kanno, K. Sugisaki, H. Nakamura, H. Yamauchi, R. Sakuma, T. Kobayashi, Q. Gao, and N. Yamamoto, arXiv [quant-ph] (2024), 2408.04946.